Title

The Role of Interferon-γ in Autoimmune Polyendocrine Syndrome Type 1.

Journal

New England Journal of Medicine, 390(20)

Authors

Oikonomou, Vasileios
Smith, Grace
Constantine, Gregory
et al.

Publication Date

2024-05-30

DOI

10.1056/NEJMoa2312665

Peer reviewed

HHS Public Access

Author manuscript

N Engl J Med. Author manuscript; available in PMC 2024 November 30.

Published in final edited form as:

N Engl J Med. 2024 May 30; 390(20): 1873–1884. doi:10.1056/NEJMoa2312665.

The Role of Interferon-γ in Autoimmune Polyendocrine Syndrome Type 1

A full list of authors and affiliations appears at the end of the article.

Abstract

BACKGROUND—Autoimmune polyendocrine syndrome type 1 (APS-1) is a life-threatening, autosomal recessive syndrome caused by autoimmune regulator (AIRE) deficiency. In APS-1, self-reactive T cells escape thymic negative selection, infiltrate organs, and drive autoimmune injury. The effector mechanisms governing T-cell–mediated damage in APS-1 remain poorly understood.

METHODS—We examined whether APS-1 could be classified as a disease mediated by interferon-γ. We first assessed patients with APS-1 who were participating in a prospective natural history study and evaluated mRNA and protein expression in blood and tissues. We then examined the pathogenic role of interferon-γ using *Aire*$^{-/-}$*Ifng*$^{-/-}$ mice and *Aire*$^{-/-}$ mice treated with the Janus kinase (JAK) inhibitor ruxolitinib. On the basis of our findings, we used ruxolitinib to treat five patients with APS-1 and assessed clinical, immunologic, histologic, transcriptional, and autoantibody responses.

RESULTS—Patients with APS-1 had enhanced interferon-γ responses in blood and in all examined autoimmunity-affected tissues. *Aire*$^{-/-}$ mice had selectively increased interferon-γ production by T cells and enhanced interferon-γ, phosphorylated signal transducer and activator of transcription 1 (pSTAT1), and CXCL9 signals in multiple organs. *Ifng* ablation or ruxolitinib-induced JAK–STAT blockade in *Aire*$^{-/-}$ mice normalized interferon-γ responses and averted T-cell infiltration and damage in organs. Ruxolitinib treatment of five patients with APS-1 led to decreased levels of T-cell–derived interferon-γ, normalized interferon-γ and CXCL9 levels, and remission of alopecia, oral candidiasis, nail dystrophy, gastritis, enteritis, arthritis, Sjögren's-like syndrome, urticaria, and thyroiditis. No serious adverse effects from ruxolitinib were identified in these patients.

CONCLUSIONS—Our findings indicate that APS-1, which is caused by AIRE deficiency, is characterized by excessive, multiorgan interferon-γ–mediated responses. JAK inhibition with

---

Disclosure forms provided by the authors are available with the full text of this article at NEJM.org.

The authors' full names, academic degrees, and affiliations are listed in the Appendix. Dr. Lionakis can be contacted at lionakism@mail.nih.gov or at the Laboratory of Clinical Immunology and Microbiology, National Institute of Allergy and Infectious Diseases, National Institutes of Health, Bldg. 10, Rm. 12C103A, MSC 1888, 10 Center Dr., Bethesda, MD 20892–1888.

Drs. Siefert, Ghosh, and Walkiewicz serve as authors on behalf of the NIAID Centralized Sequencing Program. Dr. Martin serves as an author on behalf of the Genomics and Computational Biology Core. A complete list of the members of the Genomics and Computational Biology Core and NIAID Centralized Sequencing Program is provided in the Supplementary Appendix, available at NEJM.org.

Dr. Oikonomou and Ms. Smith and Dr. Constantine, Ms. Schmitt, Ms. Ferré, and Ms. Alejo contributed equally to this article.

ruxolitinib in five patients showed promising results. (Funded by the National Institute of Allergy and Infectious Diseases and others.)

AUTOIMMUNE POLYENDOCRINE SYNdrome type 1 (APS-1), also known as autoimmune polyendocrinopathy, candidiasis, and ectodermal dystrophy (APECED), is an autosomal recessive multiorgan syndrome caused by loss-of-function variants in *AIRE*, the gene encoding autoimmune regulator.[1–3] APS-1 manifests in childhood with a characteristic triad of chronic mucocutaneous candidiasis, adrenal insufficiency, and hypoparathyroidism, alongside numerous other endocrine and nonendocrine diseases.[4–7] Mortality can exceed 30% despite supportive care.[8] Although progress has been made in the treatment of certain tissue-specific autoimmune manifestations,[9] no therapy targets the multiorgan nature of APS-1.

AIRE drives the thymic expression of tissue-restricted antigens that facilitate the negative selection of self-reactive T cells and central tolerance.[3,10] In AIRE deficiency, self-reactive T cells escape to the periphery, infiltrate organs, and drive autoimmune damage.[10–14] We performed exploratory studies involving patients with APS-1 and used $Aire^{-/-}$ mice to study mechanisms of T-cell–mediated tissue injury and to test therapeutic strategies. On the basis of these findings, which suggested that APS-1 is an interferon-γ–mediated disease, we used ruxolitinib, a Food and Drug Administration (FDA)–approved Janus kinase (JAK) 1 and 2 inhibitor,[15–17] to treat five patients with APS-1. These observations provide new insights into the mechanism and pathophysiological basis of APS-1 and uncover important targets for therapeutic intervention.

METHODS

STUDY SAMPLE

We conducted an institutional review board (IRB)–approved, prospective, observational, natural history study involving a cohort of 110 adult and pediatric patients with APS-1 from a National Institutes of Health (NIH)–sponsored international umbrella study of fungal infections (ClinicalTrials.gov number, NCT01386437; see the protocol and the Supplementary Appendix, available with the full text of this article at NEJM.org). All patients provided written informed consent before participating in the study. Our study cohort was largely representative of patients with APS-1 (Table S10 in the Supplementary Appendix). Our study also included assessments of wild-type and $Aire^{-/-}$ animals.

No commercial entity played a role in the study design or execution. The authors vouch for the accuracy and completeness of the data and the fidelity of the study to the protocol.

EXPLORATORY SEROLOGIC AND HISTOLOGIC STUDIES IN PATIENTS WITH APS-1

We conducted transcriptional analyses of peripheral-blood mononuclear cells (PBMCs) and enzyme-linked immunosorbent assay, autoantibody, and proteomic analyses of serum from adults and children in our cohort of patients with APS-1. Selected patients underwent clinically indicated diagnostic procedures, and leftover tissue-biopsy materials were used

for histologic, immunohistochemical, in situ hybridization, and RNA-sequencing analyses aimed at evaluating interferon-γ responses. All the patients who underwent procedures were included in our analysis (Tables S1 through S3). Data for comparative analyses were obtained from healthy adult donors enrolled in IRB-approved research studies in which blood and tissues were harvested. Sampling constraints made matching of patient and healthy donor samples infeasible for most comparisons.

HYPOTHESIS-DRIVEN STUDIES IN MICE AND RATS

To corroborate the interferon-γ responses found in patients with APS-1, we performed immunologic evaluations of wild-type and *Aire*$^{-/-}$ mice and in situ hybridization evaluations of wild-type and *Aire*$^{-/-}$ rats. *Ifng* ablation and ruxolitinib treatment of *Aire*$^{-/-}$ mice were used in clinical, histologic, and immunologic evaluations to test the hypothesis that enhanced interferon-γ responses drive the autoimmune damage of AIRE deficiency.

PILOT OBSERVATIONAL INTERVENTIONAL STUDY OF RUXOLITINIB IN PATIENTS WITH APS-1

Five patients with APS-1 and severe autoimmunity received ruxolitinib, which was supplied by the NIH Clinical Center Pharmacy. These patients underwent clinical, histologic, flow-cytometric, and RNA-sequencing evaluations.

STATISTICAL ANALYSIS

No samples were excluded from the analyses, which were performed with the use of a two-tailed unpaired t-test or a two-tailed Mann–Whitney test. Mean and median differences with 95% confidence intervals were obtained for parametric and nonparametric tests, respectively. Although some end-point assessments included adjustment for multiple comparisons by means of an analysis of variance test with Bonferroni's or Tukey's correction (Table S4), no overall adjustment was made for the more than two dozen end points assessed. Therefore, no conclusions about statistical significance may be drawn. These are all exploratory analyses from which causal inferences cannot be made. The Supplementary Appendix provides details of the experimental and statistical methods.

RESULTS

EXACERBATED INTERFERON-γ–MEDIATED RESPONSES IN PATIENTS WITH APS-1

A survey of 180 proteins involved in immunity and inflammation in serum from 35 patients with APS-1 and 40 healthy donors identified 58 differentially expressed proteins, including several interferon-γ–regulated molecules that were enriched in patients with APS-1 (Fig. 1A and 1B). We used gene-set enrichment analysis[18] and found "the interferon-γ response" among the top-three enriched "hallmark" pathways curated within the Molecular Signatures Database[19] (Fig. 1C).

We also found increased levels of interferon-γ and interferon-γ–inducible CXCL9 and CXCL10 in serum from patients (Fig. 1D). Expression of 15 interferon-γ–regulated genes

(Table S5), as determined with the use of NanoString,[20] was enhanced in patient PBMCs, with associated increased expression of 11 nuclear factor κB–regulated genes (Fig. 1E and Fig. S1), a finding consistent with interferon-γ–induced cell priming.[21] In contrast, expression of 28 type 1 interferon–regulated genes was unchanged. Increased interferon-γ, phosphorylated signal transducer and activator of transcription 1 (pSTAT1), CXCL9, and CXCL10 were also found in bronchoalveolar lavage fluid from patients (Fig. S2).

We performed immunohistochemical and in situ hybridization–based detection of interferon-γ, pSTAT1, and CXCL9 to examine interferon-γ responses in 97 tissue samples from 40 patients, among whom 10 autoimmune manifestations were present: pneumonitis, hepatitis, gastritis, enteritis, colitis, nephritis, Sjögren's-like syndrome, chronic mucocutaneous candidiasis, APECED rash, and alopecia. All tissues had profound T-cell infiltration and interferon-γ, pSTAT1, and CXCL9 signals, which were undetectable in healthy donor tissues without inflammation (Fig. 2 and Figs. S3 and S4). Increased expression of interferon-γ–response and interleukin-17–response genes was found in the oral mucosa of patients with acute candidiasis (Fig. S5). Thus, we concluded that patients with APS-1 have exacerbated interferon-γ–mediated responses across multiple autoimmunity-affected tissues.

USE OF ANIMAL MODELS OF APS-1 TO DETERMINE INTERFERON-γ–MEDIATED DISEASE MECHANISM

We next examined whether type 1 responses were enhanced in the APS-1 animal models. We found increased CD4+ and CD8+ T-cell accumulation in *Aire*$^{-/-}$ mouse tissues (Fig. S6A).[10,12] Production of interferon-γ by CD4+ and CD8+ T cells was increased (Figs. S6B, S6C, and S7A), whereas production of type 2 and type 17 cytokines by T cells was unaffected (Fig. S8). Interferon-γ levels were also increased in *Aire*$^{-/-}$ mouse serum and tissues, whereas levels of type 2 and type 17 cytokines were not (Figs. S7B, S9A, and S10). Moreover, we found increased levels of pSTAT1, CXCL9, and CXCL10 in *Aire*$^{-/-}$ mouse and rat serum and tissues (Figs. S7C through S7E, S9B through S9D, and S11). Therefore, Aire deficiency was associated with selectively enhanced, T-cell–derived, interferon-γ–mediated responses in multiple tissues.

We generated *Aire*$^{-/-}$*Ifng*$^{-/-}$ mice and found they had 80% survival, as compared with universal mortality among *Aire*$^{-/-}$ mice (Fig. 3A and Fig. S7F); these findings indicated that interferon-γ may be a primary driver of lethal autoimmunity in AIRE deficiency, although other factors are also likely to contribute. *Aire*$^{-/-}$*Ifng*$^{-/-}$ mice were healthy-appearing and had less lymphocytic infiltration and multiorgan damage than untreated mice, as assessed by gross pathological and histologic examination (Video 1, Fig. 3A and Figs. S7G and S12 through S14).

Because interferon-γ acts through activation of JAK1 and JAK2, we reasoned that pharmacologic inhibition of JAK1 and JAK2 with ruxolitinib, which received FDA approval in 2011 and has a long-established safety and efficacy profile,[15–17] may abrogate excessive interferon-γ–mediated responses and ameliorate multiorgan autoimmunity. Ruxolitinib treatment — starting at 3 weeks of age, when *Aire*$^{-/-}$ mice already show signs of autoimmunity (Fig. S15) — decreased CD4+ and CD8+ T-cell accumulation and interferon-

γ production by T cells, whereas production of type 2 and type 17 cytokines was unaffected (Figs. S7H, S16, and S17). Concordantly, ruxolitinib normalized levels of interferon-γ, pSTAT1, CXCL9, and CXCL10 in *Aire*$^{-/-}$ mouse serum and tissues (Figs. S7I through S7L and S18).

Ruxolitinib-treated *Aire*$^{-/-}$ mice were healthy-appearing and had 100% survival, as well as decreased lymphocytic inflammation and multiorgan damage (Video 2, Fig. 3B, and Figs. S7M, S7N, and S19 through S21). Ruxolitinib also protected *Aire*$^{-/-}$ mice from oral candidiasis (Fig. S7O and S7P). Thus, interferon-γ excess may mediate the multiorgan damage of Aire deficiency, and the fact that ruxolitinib rescued *Aire*$^{-/-}$ mice from lethal autoimmunity suggested a potential mechanism-based therapeutic intervention for patients.

RUXOLITINIB AND MULTIORGAN AUTOIMMUNITY IN PATIENTS WITH APS-1

On the basis of these matching findings indicating hyperactivated interferon-γ responses in APS-1 patients and in animals, we used ruxolitinib, which is FDA-approved for several autoimmune and neoplastic disorders, to treat five patients with severe autoimmunity (Table S6).

Patient 1

Patient 1 was a 37-year-old woman from the United States who had alopecia (Fig. 4A and Fig. S22A and S22B), sicca symptoms (Fig. S22C), and autoimmune enteritis–associated severe constipation with rectal prolapse; the patient was taking 14 linaclotide pills (72 μg each) per week in order to have a bowel movement (Fig. S22D). Endoscopy revealed atrophic gastritis (Fig. S23), T-cell inflammation, and increased interferon-γ, pSTAT1, and CXCL9 levels in the stomach and duodenum (Fig. S24).

Treatment with ruxolitinib was initiated at a dose of 5 mg twice daily, and within 2 weeks, laxative use decreased and constipation abated (Fig. S25). At 1 month, the ruxolitinib dose was increased to 10 mg twice daily, and linaclotide use was reduced further. One month later, the ruxolitinib dose was increased to 20 mg twice daily, and within 2 weeks, scalp and eyebrow hair began growing, with eventual complete scalp, eyelash, and eyebrow hair regrowth over 10 weeks (Fig. 4A and Fig. S22A and S22B). The sicca symptoms abated, salivary flow normalized (Fig. S22C), linaclotide use further decreased (Fig. S22D), bowel movements normalized, and arthritis symptoms and nail dystrophy decreased. One month later, mild exertional dyspnea developed. Evaluation revealed anemia (hemoglobin level, 8 mg per deciliter), possibly from ruxolitinib-induced erythropoiesis inhibition, and normoxemia (oxygen saturation [Spo_2], 98%), and induced sputum was polymerase chain reaction–positive and direct fluorescent antibody–negative for *Pneumocystis jirovecii*. Treatment with ruxolitinib was paused, atovaquone prophylaxis was initiated, and red cells were transfused, after which the hemoglobin level returned to baseline (approximately 10 mg per deciliter); ruxolitinib treatment was restarted at 15 mg twice daily without further adverse effects. Serum interferon-γ and CXCL9 levels and T-cell–derived interferon-γ production decreased (Fig. 4A and Fig. S22E through S22G). Alopecia, enteritis, Sjögren's-

like syndrome, nail dystrophy, and arthritis remained in remission without toxic effects. One year after the initiation of ruxolitinib treatment, endoscopy showed resolution of atrophic gastritis (Fig. S23) with decreased gastric and duodenal lymphocytic infiltration and decreased interferon-γ, pSTAT1, and CXCL9 signals (Fig. S24). Remission was associated with unaltered cytokine-targeted or organ-specific autoantibodies and a decrease in percentages of CD8+ T cells within peripheral blood (Fig. S26 and Tables S7 and S8).

Patient 2

Patient 2 was a 45-year-old man from the United States who had end-stage renal disease and autoimmune enteritis–associated diarrhea, fat malabsorption, and bowel movements that contained undigested food (Fig. S22H through S22K). He could not gain weight (Fig. S22L and S22M). He had recurrent oral candidiasis, with three episodes per year treated with fluconazole (Fig. S22N). Endoscopy revealed severe atrophic gastritis, T-cell infiltration, and increased gastric and duodenal levels of interferon-γ, pSTAT1, and CXCL9 (Fig. 4B and Figs. S22O, S22P, and S27).

Treatment with ruxolitinib was initiated at a dose of 5 mg three times per week after hemodialysis; within 4 weeks, diarrhea had abated (Fig. S25). At 1 month, the ruxolitinib dose was increased to 10 mg three times per week. Diarrhea and undigested food–containing bowel movements resolved. Although the patient decided to discontinue levothyroxine treatment at month 2, levels of thyroid-stimulating hormone remained normal while he was receiving ruxolitinib (Fig. S22Q). His eyelashes regrew. At 7 months, the ruxolitinib dose was increased to 15 mg three times per week. Serum levels of interferon-γ and CXCL9 normalized, T-cell–derived interferon-γ production decreased (Fig. 4B and Fig. S22R through S22T), his weight increased (Fig. S22L and S22M), and facial hair grew, which allowed the patient to shave for the first time in his life. At 1 year, his bowel movements remained normal, and fecal fat levels had normalized (Fig. S22H through S22K). No oral candidiasis developed during the year in which he was receiving ruxolitinib (Fig. S22N); candidiasis remission was associated with decreased interferon-γ response gene expression in the oral mucosa without accompanying increased expression of interleukin-17 genes or a decline in T helper 17 cytokine–targeted or other autoantibodies (Figs. S26, S28, and S29 and Table S9). Endoscopy showed resolution of atrophic gastritis with reduced gastric and intestinal T-cell infiltration and interferon-γ pathway signals (Fig. 4B and Figs. S22O, S22P, and S27).

Patient 3

Patient 3 was a 12-year-old boy from Spain who had alopecia (Fig. 5A and Fig. S30A and S30B) and autoimmune enteritis–associated diarrhea, urgency, abdominal pain, bowel movements containing undigested food, nocturnal diarrhea, iron-deficiency anemia, and malnutrition (Fig. 5A and Figs. S30C through S30F and S31). His condition had not improved during previous trials of tacrolimus, sirolimus, and rituximab.

Treatment with ruxolitinib was initiated at a dose of 5 mg twice daily, and the patient had a mild decrease in diarrhea (Fig. S25). At 3 months, the dose of ruxolitinib was increased to 10 mg twice daily, and within 3 weeks, diarrhea abated. Within 2 months

after the dose increase, the number and consistency of bowel movements normalized (Fig. S30C and S30D). Episodes of nocturnal diarrhea, undigested food–containing bowel movements, and associated abdominal pain and urgency resolved, and the fecal calprotectin level decreased; in addition, the hemoglobin level and transferrin saturation increased, and iron supplementation was discontinued (Fig. S31). His weight and height increased (Fig. 5A and Figs. S30E, S30F, and S32). At 9 months, his nail dystrophy abated (Fig. S33) and his scalp (Fig. 5A and Fig. S30A and S30B), eyelash, and eyebrow hair began growing, with eventual near-complete hair regrowth over 3 months. At 1 year after the initiation of ruxolitinib treatment, he remained in remission with continuously improving scalp hair regrowth and no toxic effects.

Patient 4

Patient 4 was a 15-year-old girl from Finland who had autoimmune enteritis–associated diarrhea with abdominal pain, iron-deficiency anemia treated with parenteral iron supplementation, metabolic acidosis necessitating bicarbonate administration, and malnutrition treated with partial parenteral nutrition (Fig. 5B and Fig. S30G through S30L). She had delayed puberty and growth retardation. Endoscopy showed gastric and duodenal T-cell inflammation; increased levels of interferon-γ, pSTAT1, and CXCL9; and an absence of Paneth and enteroendocrine cells (Figs. S30M, S30N, S34, and S35).[22,23]

Treatment with ruxolitinib was initiated at a dose of 5 mg twice daily, and within 2 weeks diarrhea began decreasing (Fig. S25). At 6 weeks, the number and consistency of bowel movements further improved and nocturnal diarrhea resolved. The dose of ruxolitinib was increased to 7.5 mg alternating with 5 mg, and within a few days bowel function further improved, with resolution of diarrhea and metabolic acidosis, discontinuation of bicarbonate supplementation, and eventual resolution of abdominal pain (Fig. 5B and Fig. S30G through S30I). Two months after the initiation of ruxolitinib treatment, the patient reached puberty, and at 4 months, vitamin E supplementation and partial parenteral nutrition were discontinued. Her anemia abated without the need for iron infusions (Fig. S30J). Her weight increased (Fig. 5B and Fig. S30K and S30L). Her exocrine pancreatic insufficiency abated, as evidenced by reductions in the dose of pancrelipase and increases in the vitamin E and fecal elastase 1 levels (Fig. S36). At 9 months, endoscopy showed decreased lymphocytic infiltration and decreased interferon-γ pathway signals with Paneth and enteroendocrine cell restoration (Figs. S30M, S30N, S34, and S35). At 1 year after the initiation of ruxolitinib treatment, the patient remained in remission without toxic effects.

Patient 5

Patient 5 was an 11-year-old girl from Bosnia and Herzegovina who had severe autoimmune enteritis–associated constipation and abdominal pain and distention. She took multiple laxatives and enemas to facilitate a bowel movement, which culminated in numerous hospitalizations, totaling 23 days over a period of 6 months (Fig. S30O through S30R). This adversely affected her school attendance, recorded on 40% of open school days (Fig. S30S). She was malnourished (Fig. 5C and Fig. S30T and S30U) and had anti-histamine-refractory urticaria and recurrent oral candidiasis, with an average of three episodes per year treated with fluconazole. Endoscopy revealed gastric and duodenal T-cell infiltration, increased

interferon-γ pathway signals, and reduced presence of enteroendocrine cells (Figs. S37 and S38).

Ruxolitinib was initiated at a dose of 5 mg twice daily, and within 1 month, her use of laxatives decreased, stool consistency improved, constipation abated, and abdominal pain and distention resolved (Fig. S25). By 3 months, her bowel function had further improved and her use of laxatives and enemas had further decreased. At that time, the dose of ruxolitinib was increased to 10 mg twice daily. Over the next 3 months, the serum interferon-γ and CXCL10 levels diminished, bowel function normalized, laxatives and enemas were discontinued, and weight increased (Fig. 5C and Figs. S30O through S30Q, S30T through S30V, and S39). Since starting ruxolitinib treatment, she had not been hospitalized for constipation and was able to attend school normally (Fig. S30R and S30S). Although an isolated episode of oral candidiasis occurred at the onset of the 5-mg twice-daily ruxolitinib administration, no subsequent episodes occurred. Urticaria symptoms ceased, and antihistamines were stopped (Fig. S39). At 8 months after the initiation of ruxolitinib treatment, the patient remained in remission without toxic effects.

Discussion

We identified excessive interferon-γ production by AIRE-deficient T cells as a critical pathogenic mechanism underlying autoimmune multiorgan injury and observed therapeutic benefits of JAK inhibition in both mouse models and patients with APS-1. These findings support APS-1 as an “interferon-gammopathy” and provide new insights into the pathogenesis and treatment of autoimmunity caused by impaired central tolerance. These are new potential targets for therapeutic intervention that need to be studied further in clinical trials.

T-cell depletion and adoptive transfer experiments have shown that AIRE-deficient T cells are necessary and sufficient to promote autoimmune injury.[10–14] We found exacerbated interferon-γ–mediated responses in blood and multiple tissues of patients with APS-1.[6] Similarly, we found selectively increased interferon-γ production by AIRE-deficient T cells and enhanced interferon-γ responses in *Aire*$^{-/-}$ mice.[11,12,24,25] This interferon-γ excess appeared to underlie the multiorgan damage of Aire deficiency in mice, as indicated by the fact that *Ifng* ablation or ruxolitinib-mediated JAK–STAT inhibition downstream of interferon-γ–interferon-γ receptor engagement reduced interferon-γ production, interferon-γ–mediated responses, T-cell infiltration, and tissue damage and averted lethal autoimmunity in *Aire*$^{-/-}$ mice.

On the basis of this biologic evidence from patients with APS-1 and the APS-1 animal model, we used ruxolitinib, which is FDA-approved for myelofibrosis, polycythemia vera, vitiligo, and graft-versus-host disease; we chose this drug because of its long-standing clinical experience, relative to that of other JAK or interferon-γ inhibitors, and its remarkable efficacy in *Aire*$^{-/-}$ mice. Long-term ruxolitinib treatment was associated with remission of conditions such as alopecia, oral candidiasis, nail dystrophy, gastritis, enteritis, arthritis, Sjögren’s-like syndrome, urticaria, and thyroiditis. Of note was the remission of severe enteritis with malabsorption, malnutrition, acidosis, anemia, or delayed puberty

(or a combination of these conditions) in three children; remission of oral candidiasis, which expands our previous observations[11]; and remission of gastritis, Sjögren's syndrome, and thyroiditis, which are autoimmune disorders for which effective immunomodulatory treatments have not been well established. Whether JAK inhibitors may have a role in these disorders beyond APS-1 merits exploration, in light of their expanding indications in rheumatologic, gastrointestinal, dermatologic, and atopic conditions.

Ruxolitinib abrogated excessive interferon-γ–mediated responses by inhibiting T-cell–derived interferon-γ production and blocking downstream interferon-γ–mediated signals[26,27]; it also reduced T-cell infiltration without overtly altering autoantibodies. Future studies should examine the potential contribution of other JAK-dependent type 1 immune effectors beyond interferon-γ in these responses (e.g., interleukin-2, interleukin-12, and tumor necrosis factor α)[12,28] and determine the efficacy of ruxolitinib relative to other JAK1 and JAK2 inhibitors (e.g., tofacitinib or baricitinib), JAK1-selective inhibitors, and the recently approved interferon-γ–targeted emapalumab in APS-1. Remission in all five patients with APS-1 was achieved with ruxolitinib doses that were substantially lower than the maximal FDA-approved dose of 25 mg twice daily, which may suggest a wider therapeutic index in APS-1 and may help to avoid toxic effects.

Our study has limitations, including the imperfect matching of healthy donors to patients with APS-1 and the small number of ruxolitinib-treated patients. Treatment in a clinical trial is needed to further clarify the efficacy and long-term safety of ruxolitinib in patients with APS-1 as well as the dose to be used in these patients.

Our study suggests that excessive interferon-γ–mediated responses have a pathogenic role in APS-1 and provides the foundation for therapies that affect interferon-γ–mediated disease.

Supported by the Division of Intramural Research of the National Institute of Allergy and Infectious Diseases (NIAID), the National Cancer Institute, the National Institute of Arthritis and Musculoskeletal and Skin Diseases, the National Heart, Lung, and Blood Institute, the National Institute of Dental and Craniofacial Research, the National Institutes of Health (NIH) Clinical Center, and the National Institute of Diabetes and Digestive and Kidney Diseases — all part of the NIH.

Supplementary Material

Refer to Web version on PubMed Central for supplementary material.

Authors

Vasileios Oikonomou, Ph.D.,
Grace Smith, B.S.,
Gregory M. Constantine, M.D.,
Monica M. Schmitt, C.R.N.P.,
Elise M.N. Ferré, P.A.-C., M.P.H.,
Julie C. Alejo, B.S.,
Deanna Riley, B.S.,

Dhaneshwar Kumar, Ph.D.,
Lucas Dos Santos Dias, Ph.D.,
Joseph Pechacek, M.D.,
Yannis Hadjiyannis, M.D.,
Taura Webb, C.R.N.P.,
Bryce A. Seifert, Ph.D.,
Rajarshi Ghosh, Ph.D.,
Magdalena Walkiewicz, Ph.D.,
Daniel Martin, Ph.D.,
Marine Besnard, Ph.D.,
Brendan D. Snarr, Ph.D.,
Shiva Deljookorani, B.S.,
Chyi-chia R. Lee, M.D.,
Tom DiMaggio, R.N.,
Princess Barber, R.N.,
Lindsey B. Rosen, Ph.D.,
Aristine Cheng, M.D.,
Andre Rastegar, B.S.,
Adriana A. de Jesus, M.D.,
Jennifer Stoddard, B.S.,
Hye Sun Kuehn, Ph.D.,
Timothy J. Break, Ph.D.,
Heidi H. Kong, M.D., M.H.Sc.,
Leslie Castelo-Soccio, M.D., Ph.D.,
Ben Colton, Pharm.D.,
Blake M. Warner, D.D.S., Ph.D., M.P.H.,
David E. Kleiner, M.D.,
Martha M. Quezado, M.D.,
Jeremy L. Davis, M.D.,
Kevin P. Fennelly, M.D.,
Kenneth N. Olivier, M.D.,
Sergio D. Rosenzweig, M.D., Ph.D.,
Anthony F. Suffredini, M.D.,
Mark S. Anderson, M.D., Ph.D.,
Marc Swidergall, Ph.D.,
Carole Guillonneau, Ph.D.,
Luigi D. Notarangelo, M.D.,
Raphaela Goldbach-Mansky, M.D.,
Olaf Neth, M.D., Ph.D.,

Maria Teresa Monserrat-Garcia, M.D.,
Justo Valverde-Fernandez, M.D.,
Jose Manuel Lucena, Ph.D.,
Ana Lucia Gomez-Gila, M.D.,
Angela Garcia Rojas, M.D.,
Mikko R. J. Seppänen, M.D.,
Jouko Lohi, M.D., Sc.D.,
Matti Hero, M.D.,
Saila Laakso, M.D.,
Paula Klemetti, M.D.,
Vanja Lundberg, M.D., Ph.D.,
Olov Ekwall, M.D., Ph.D.,
Peter Olbrich, M.D., Ph.D.,
Karen K. Winer, M.D.,
Behdad Afzali, M.D., Ph.D.,
Niki M. Moutsopoulos, D.D.S., Ph.D.,
Steven M. Holland, M.D.,
Theo Heller, M.D.,
Stefania Pittaluga, M.D., Ph.D.,
Michail S. Lionakis, M.D., Sc.D.

Affiliations

Acknowledgments

We thank our patients and their families for their participation in our study; the NIAID clinical fellows, residents, and nursing staff of the inpatient wards and outpatient clinics for their dedication to patient care; Andrew Wishart, Muthulekha Swamydas, and Teresa Greenwell-Wild for technical assistance; and Laurie Brenchley for assistance with clinical research evaluations.

APPENDIX

The authors' full names and academic degrees are as follows: Vasileios Oikonomou, Ph.D., Grace Smith, B.S., Gregory M. Constantine, M.D., Monica M. Schmitt, C.R.N.P., Elise M.N. Ferré, P.A.-C., M.P.H., Julie C. Alejo, B.S., Deanna Riley, B.S., Dhaneshwar Kumar, Ph.D., Lucas Dos Santos Dias, Ph.D., Joseph Pechacek, M.D., Yannis Hadjiyannis, M.D., Taura Webb, C.R.N.P., Bryce A. Seifert, Ph.D., Rajarshi Ghosh, Ph.D., Magdalena Walkiewicz, Ph.D., Daniel Martin, Ph.D., Marine Besnard, Ph.D., Brendan D. Snarr, Ph.D., Shiva Deljookorani, B.S., Chyi-chia R. Lee, M.D., Tom DiMaggio, R.N., Princess Barber, R.N., Lindsey B. Rosen, Ph.D., Aristine Cheng, M.D., Andre Rastegar, B.S., Adriana A. de Jesus, M.D., Jennifer Stoddard, B.S., Hye Sun Kuehn, Ph.D., Timothy J. Break, Ph.D., Heidi H. Kong, M.D., M.H.Sc., Leslie Castelo-Soccio, M.D., Ph.D., Ben Colton, Pharm.D., Blake M. Warner, D.D.S., Ph.D., M.P.H., David E. Kleiner, M.D., Martha M. Quezado, M.D., Jeremy L. Davis, M.D., Kevin P. Fennelly, M.D., Kenneth N. Olivier, M.D., Sergio

D. Rosenzweig, M.D., Ph.D., Anthony F. Suffredini, M.D., Mark S. Anderson, M.D., Ph.D., Marc Swidergall, Ph.D., Carole Guillonneau, Ph.D., Luigi D. Notarangelo, M.D., Raphaela Goldbach-Mansky, M.D., Olaf Neth, M.D., Ph.D., Maria Teresa Monserrat-Garcia, M.D., Justo Valverde-Fernandez, M.D., Jose Manuel Lucena, Ph.D., Ana Lucia Gomez-Gila, M.D., Angela Garcia Rojas, M.D., Mikko R. J. Seppänen, M.D., Jouko Lohi, M.D., Sc.D., Matti Hero, M.D., Saila Laakso, M.D., Paula Klemetti, M.D., Vanja Lundberg, M.D., Ph.D., Olov Ekwall, M.D., Ph.D., Peter Olbrich, M.D., Ph.D., Karen K. Winer, M.D., Behdad Afzali, M.D., Ph.D., Niki M. Moutsopoulos, D.D.S., Ph.D., Steven M. Holland, M.D., Theo Heller, M.D., Stefania Pittaluga, M.D., Ph.D., and Michail S. Lionakis, M.D., Sc.D.

REFERENCES

1. Oftedal BE, Hellesen A, Erichsen MM, et al. Dominant mutations in the autoimmune regulator AIRE are associated with common organ-specific autoimmune diseases. Immunity 2015;42:1185–96. [PubMed: 26084028]
2. Ricotta EE, Ferré EMN, Schmitt MM, DiMaggio T, Lionakis MS. Prevalence of APECED-like clinical disease in an electronic health record database, USA. J Clin Immunol 2022;42:904–6. [PubMed: 35312911]
3. Constantine GM, Lionakis MS. Lessons from primary immunodeficiencies: autoimmune regulator and autoimmune polyendocrinopathy-candidiasis-ectodermal dystrophy. Immunol Rev 2019;287:103–20. [PubMed: 30565240]
4. Ahonen P, Myllärniemi S, Sipilä I, Perheentupa J. Clinical variation of autoimmune polyendocrinopathy-candidiasis-ectodermal dystrophy (APECED) in a series of 68 patients. N Engl J Med 1990;322:1829–36. [PubMed: 2348835]
5. Bruserud Ø, Oftedal BE, Landegren N, et al. A longitudinal follow-up of autoimmune polyendocrine syndrome type 1. J Clin Endocrinol Metab 2016;101:2975–83. [PubMed: 27253668]
6. Ferre EMN, Rose SR, Rosenzweig SD, et al. Redefined clinical features and diagnostic criteria in autoimmune polyendocrinopathy-candidiasis-ectodermal dystrophy. JCI Insight 2016;1(13):e88782.
7. Garelli S, Dalla Costa M, Sabbadin C, et al. Autoimmune polyendocrine syndrome type 1: an Italian survey on 158 patients. J Endocrinol Invest 2021;44: 2493–510. [PubMed: 34003463]
8. Borchers J, Pukkala E, Mäkitie O, Laakso S. Patients with APECED have increased early mortality due to endocrine causes, malignancies and infections. J Clin Endocrinol Metab 2020;105(6):e2207–e2213. [PubMed: 32185376]
9. Ferré EMN, Break TJ, Burbelo PD, et al. Lymphocyte-driven regional immunopathology in pneumonitis caused by impaired central immune tolerance. Sci Transl Med 2019;11(495):eaav5597.
10. Anderson MS, Venanzi ES, Klein L, et al. Projection of an immunological self shadow within the thymus by the aire protein. Science 2002;298:1395–401. [PubMed: 12376594]
11. Break TJ, Oikonomou V, Dutzan N, et al. Aberrant type 1 immunity drives susceptibility to mucosal fungal infections. Science 2021;371(6526):eaay5731.
12. Devoss JJ, Shum AK, Johannes KPA, et al. Effector mechanisms of the autoimmune syndrome in the murine model of autoimmune polyglandular syndrome type 1. J Immunol 2008;181:4072–9. [PubMed: 18768863]
13. Gavanescu I, Benoist C, Mathis D. B cells are required for Aire-deficient mice to develop multi-organ autoinflammation: a therapeutic approach for APECED patients. Proc Natl Acad Sci U S A 2008; 105:13009–14. [PubMed: 18755889]
14. Niki S, Oshikawa K, Mouri Y, et al. Alteration of intra-pancreatic target-organ specificity by abrogation of Aire in NOD mice. J Clin Invest 2006;116:1292–301. [PubMed: 16628255]
15. Vannucchi AM, Kiladjian JJ, Griess-hammer M, et al. Ruxolitinib versus standard therapy for the treatment of polycythemia vera. N Engl J Med 2015;372:426–35. [PubMed: 25629741]
16. Verstovsek S, Mesa RA, Gotlib J, et al. A double-blind, placebo-controlled trial of ruxolitinib for myelofibrosis. N Engl J Med 2012;366:799–807. [PubMed: 22375971]

17. Zeiser R, Polverelli N, Ram R, et al. Ruxolitinib for glucocorticoid-refractory chronic graft-versus-host disease. N Engl J Med 2021;385:228–38. [PubMed: 34260836]
18. Subramanian A, Tamayo P, Mootha VK, et al. Gene set enrichment analysis: a knowledge-based approach for interpreting genome-wide expression profiles. Proc Natl Acad Sci U S A 2005;102:15545–50. [PubMed: 16199517]
19. Liberzon A, Birger C, Thorvaldsdóttir H, Ghandi M, Mesirov JP, Tamayo P. The Molecular Signatures Database (MSigDB) hallmark gene set collection. Cell Syst 2015;1:417–25. [PubMed: 26771021]
20. de Jesus AA, Hou Y, Brooks S, et al. Distinct interferon signatures and cytokine patterns define additional systemic autoinflammatory diseases. J Clin Invest 2020;130:1669–82. [PubMed: 31874111]
21. Kang K, Bachu M, Park SH, et al. IFN-γ selectively suppresses a subset of TLR4-activated genes and enhancers to potentiate macrophage activation. Nat Commun 2019;10:3320. [PubMed: 31346169]
22. Dobeš J, Neuwirth A, Dobešová M, et al. Gastrointestinal autoimmunity associated with loss of central tolerance to enteric α-defensins. Gastroenterology 2015; 149:139–50. [PubMed: 25982289]
23. Posovszky C, Lahr G, von Schnurbein J, et al. Loss of enteroendocrine cells in autoimmune-polyendocrine-candidiasis-ectodermal-dystrophy (APECED) syndrome with gastrointestinal dysfunction. J Clin Endocrinol Metab 2012;97(2):E292–E300. [PubMed: 22162465]
24. Heng JS, Hackett SF, Stein-O'Brien GL, et al. Comprehensive analysis of a mouse model of spontaneous uveoretinitis using single-cell RNA sequencing. Proc Natl Acad Sci U S A 2019;116:26734–44 [PubMed: 31843893]
25. Maglakelidze N, Gao T, Feehan RP, Hobbs RP. AIRE deficiency leads to the development of alopecia areata-like lesions in mice. J Invest Dermatol 2023; 143(4):578–587.e3. [PubMed: 36270546]
26. Lee J-Y, Kim SH, Lee S-H, Kim H-R, Min HK. Effect of Janus kinase inhibitors on T cell responses to herpes zoster in rheumatoid arthritis patients. Clin Exp Rheumatol 2023;41:1077–87. [PubMed: 36062760]
27. Maeshima K, Yamaoka K, Kubo S, et al. The JAK inhibitor tofacitinib regulates synovitis through inhibition of interferon-γ and interleukin-17 production by human CD4+ T cells. Arthritis Rheum 2012;64:1790–8. [PubMed: 22147632]
28. Wang Y, Guo L, Yin X, et al. Pathogenic TNF-α drives peripheral nerve inflammation in an Aire-deficient model of autoimmunity. Proc Natl Acad Sci U S A 2022;119(4):e2114406119.

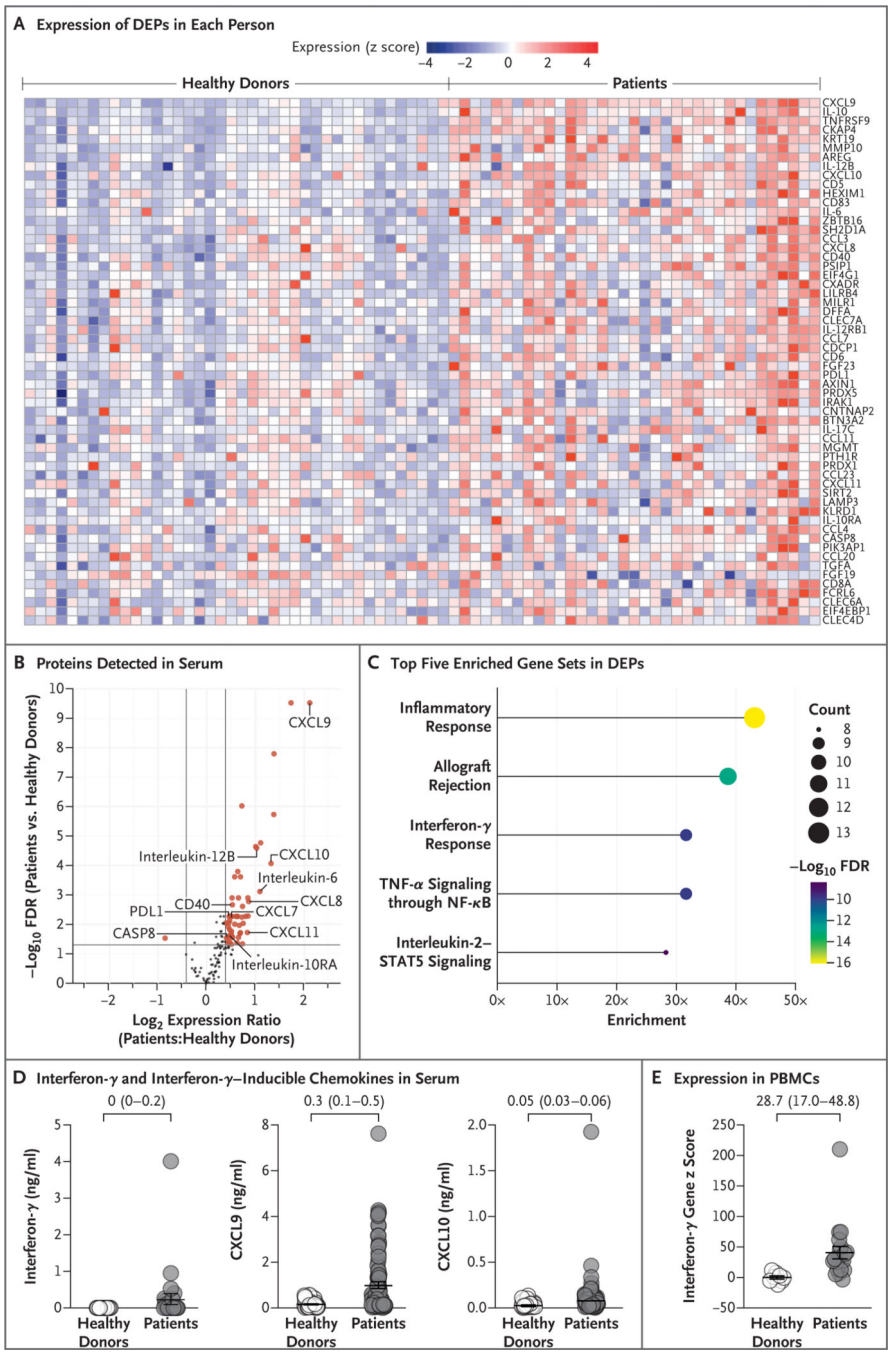

Figure 1 (facing page). Interferon-γ–Mediated Responses in Blood from Patients with APS-1.
Panels A through C show proximity extension assay–based surveys of 180 proteins, performed with serum from 35 patients with autoimmune polyendocrine syndrome type 1 (APS-1) and 40 healthy donors. Panel A is a heat map showing expression of each of the 58 differentially expressed proteins (DEPs) in each person. Red and blue indicate high and low expression, respectively; expression (expressed as the z score) ranges from −4 to 4. Panel B is a volcano plot comparing the serum proteins detected in patients with APS-1 as compared with healthy donors. Red data points are DEPs — that is, proteins with a $\log_2$

ratio of expression (patients:healthy donors) of greater than 0.4 or less than −0.4 (i.e., falling outside the area of the graph delineated by the two gray vertical lines) at a false discovery rate (FDR) of less than 0.05 (i.e., falling above the gray horizontal line). Select interferon-γ–regulated genes are labeled. Panel C shows the top five enriched Molecular Signatures Database "hallmark" gene sets in DEPs from Panel A. Colors indicate the $-\log_{10}$ FDR value, and the size of the data point indicates the gene count. The x axis shows the factor by which expression was higher in patients (e.g., 30 indicates 30 times as high in patients as in healthy donors). NF-κB denotes nuclear factor κB, and TNF-α tumor necrosis factor α. Panel D shows levels of interferon-γ and interferon-γ–inducible chemokines CXCL9 and CXCL10 in the serum of 28 to 86 patients with APS-1 and 20 to 47 healthy donors. Panel E shows expression of 15 interferon-γ–regulated genes in peripheral-blood mononuclear cells (PBMCs) of 20 patients with APS-1 and 8 healthy donors, measured by NanoString and expressed as z scores. Long horizontal bars indicate the means, and I bars indicate the standard errors. The numbers above each graph are median differences and 95% confidence intervals derived from the Mann–Whitney test. The confidence intervals were not adjusted for multiplicity and should not be used in place of hypothesis testing.

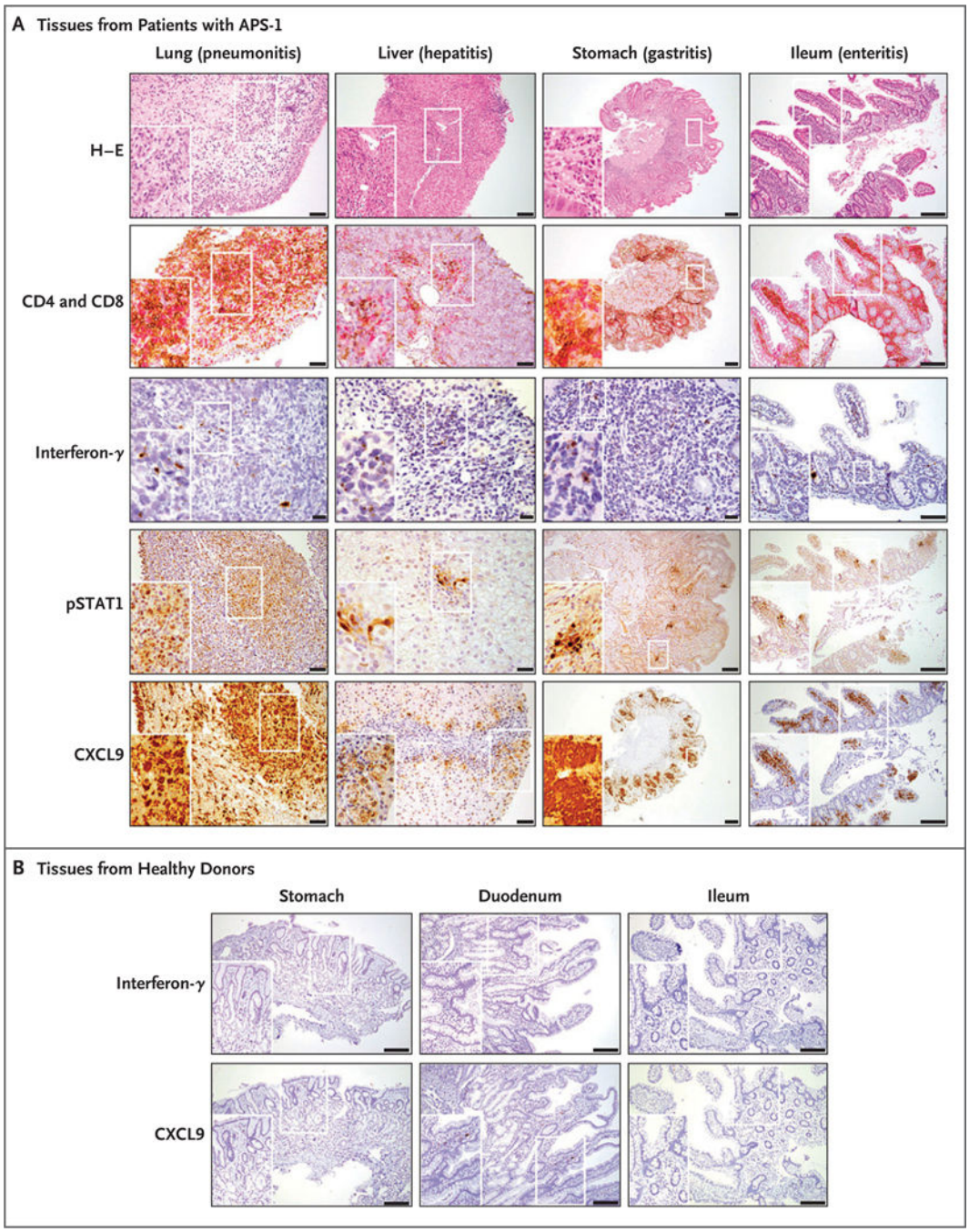

Figure 2 (facing page). . T-Cell Infiltration and Interferon-γ Pathway Signals in Multiple Autoimmunity-Affected Tissues of Patients with APS-1.

Panel A shows representative images of hematoxylin and eosin (H–E) staining, immunohistochemical staining with CD4 (brown) and CD8 (red), interferon-γ in situ hybridization staining, phosphorylated signal transducer and activator of transcription 1 (pSTAT1) immunohistochemical staining, and in situ hybridization staining for the interferon-γ–inducible chemokine CXCL9 in endobronchial biopsy tissue of a patient with APS-1 with autoimmune pneumonitis, liver tissue of a patient with APS-1 with autoimmune hepatitis, stomach tissue of a patient with APS-1 with autoimmune gastritis, and ileal tissue

of a patient with APS-1 with autoimmune enteritis. Scale bars in Panel A are as follows: 20 μm for interferon-γ images of lung, liver, and stomach and for the pSTAT1 image of liver; 50 μm for the H–E image of lung, CD4 and CD8 images of lung and liver, interferon-γ image of ileum, pSTAT1 image of lung, and CXCL9 images of lung and liver; 100 μm for H–E images of liver and ileum, CD4 and CD8 images of ileum, pSTAT1 images of stomach and ileum, and CXCL9 image of ileum; and 200 μm for H–E, CD4 and CD8, and CXCL9 images of stomach. Panel B shows representative images of in situ hybridization staining for interferon-γ and CXCL9 in stomach, duodenal, and ileal tissues of healthy donors. Scale bars in Panel B indicate 100 μm. In both panels, insets show magnified images of the area delineated by white rectangles.

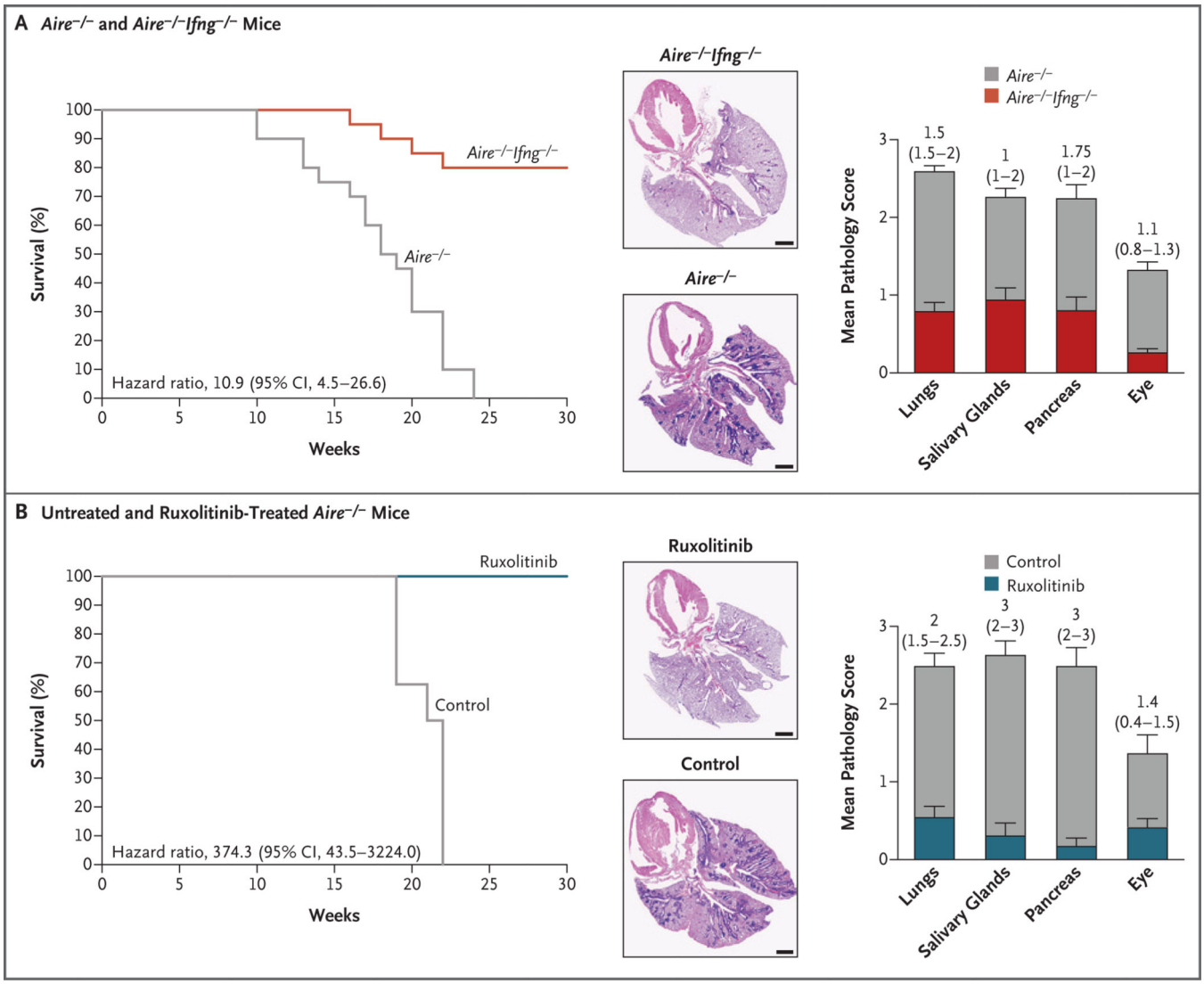

Figure 3. Survival and Organ Damage among *Aire*$^{-/-}$*Ifng*$^{-/-}$ and *Aire*$^{-/-}$ Mice with or without Ruxolitinib Treatment.

The graph in Panel A shows survival among *Aire*$^{-/-}$ and *Aire*$^{-/-}$*Ifng*$^{-/-}$ mice (20 per group). Representative hematoxylin and eosin–stained lung sections and pathology scores of the indicated tissues in 10-week-old *Aire*$^{-/-}$ and *Aire*$^{-/-}$*Ifng*$^{-/-}$ mice (27 to 31 per group) are also shown; higher pathology scores indicate more severe pathologic changes. The graph in Panel B shows survival among 8 untreated (control) and 26 ruxolitinib-treated *Aire*$^{-/-}$ mice. Representative hematoxylin and eosin–stained lung sections and pathology scores of the indicated tissues in 10-week-old *Aire*$^{-/-}$ control and ruxolitinib-treated mice (8 to 10 per group) are also shown. The scale bars in both panels indicate 1 mm. In both panels, the hazard ratios and 95% confidence intervals in the Kaplan–Meier curves were derived from the Mantel–Haenszel test, the T bars in the bar graphs indicate the standard errors, and the numbers above each bar in the bar graphs are median differences and 95% confidence intervals derived from the Mann–Whitney test. Confidence intervals were not adjusted for multiplicity and should not be used in place of hypothesis testing.

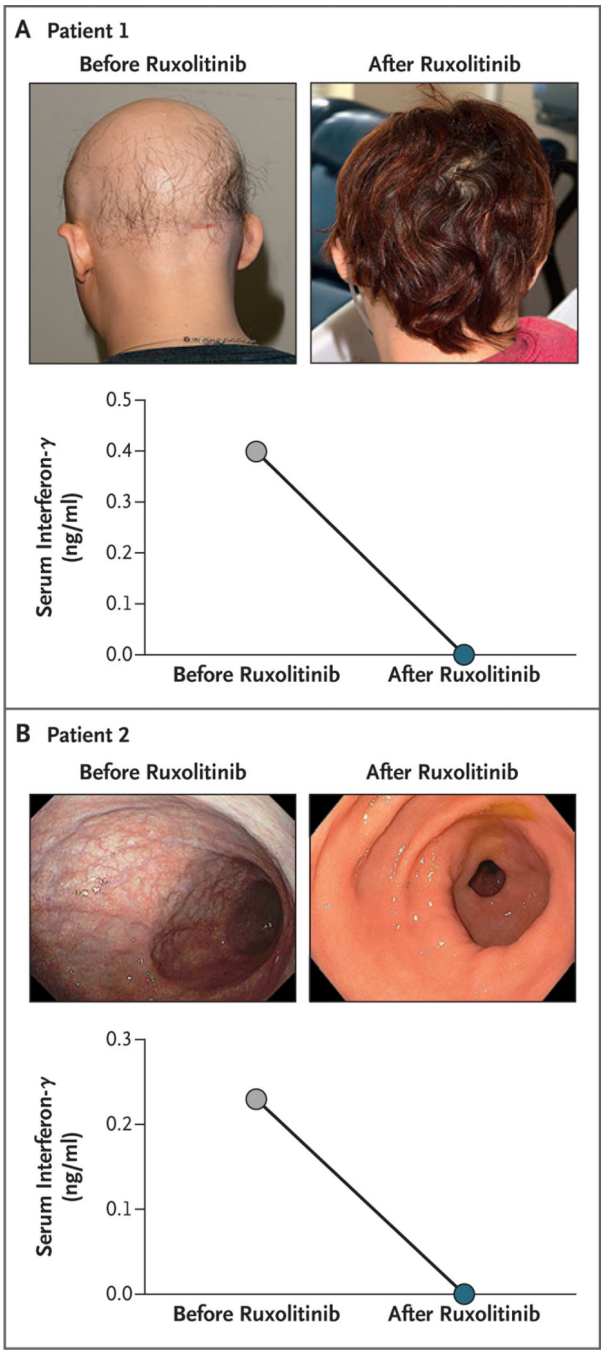

Figure 4. Ruxolitinib-Induced Remission of Autoimmune Manifestations in Patients 1 and 2.
Panel A shows photographs of hair on the scalp of Patient 1 before and after ruxolitinib treatment. The graph shows serum levels of interferon-γ before and after treatment. Panel B shows the macroscopic appearance of gastric mucosa during endoscopy in Patient 2. The graph shows serum levels of interferon-γ before and after treatment.

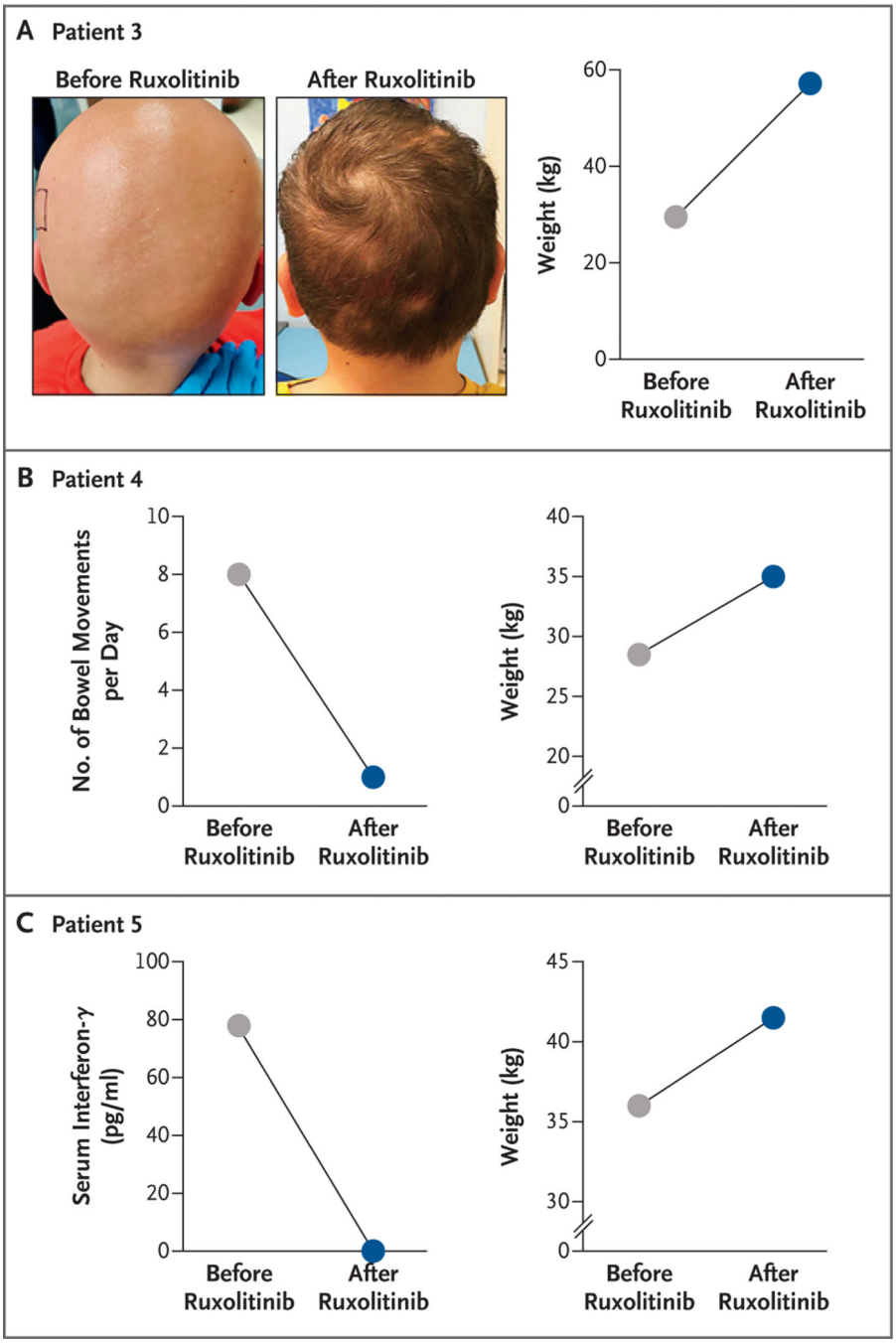

Figure 5. Ruxolitinib-Induced Remission of Autoimmune Manifestations in Patients 3, 4, and 5.
Panel A shows photographs of hair on the scalp of Patient 3 before and after ruxolitinib treatment. The graph shows the patient's change in weight after treatment. Panel B shows graphs of the number of bowel movements per day and body weight before and after treatment in Patient 4. Panel C shows graphs of body weight and serum levels of interferon-γ before and after treatment in Patient 5.